ChemComm

Overcoming the Phase Separation within High–Entropy Metal Carbide by Poly(ionic liquid)s

Journal:	*ChemComm*
Manuscript ID	CC-COM-01-2021-000497.R1
Article Type:	Communication

COMMUNICATION

Overcoming the Phase Separation within High–Entropy Metal Carbide by Poly(ionic liquid)s

Received 00th January 20xx,
Accepted 00th January 20xx

DOI: 10.1039/x0xx00000x

Yan Leng[a,b], Zihao Zhang[b], Hao Chen[b], Shengyu Du[a,c], Jixing Liu[b], Shiyang Nie[c], Yuming Dong[a], Pengfei Zhang[c]*, Sheng Dai[b,d]*

High-entropy crystalline materials are attracting more attention. In principle, high–entropy metal carbides (HMCs) that contain five or more metal ions, possess more negative free energy value during catalysis. But its preparation is challenging because of the immiscibility of multi metal cations in a single carbide solid solution. Here, a rational strategy for preparing HMC is proposed via a coordination-assisted crystallization process in the presence of Br-based poly(ionic liquids). Through this method, $Mo_{0.2}W_{0.2}V_{0.2}Cr_{0.2}Nb_{0.2}C$ nanoparticles, with a single cubic phase structure, incorporated on porous carbon, are obtained (HMC@NC). By combination of well dispersed small particle size (~4 nm), high surface area (~270 m^2/g), and high-entropy phase, HMC@NC can function as a promising catalyst for the dehydrogenation of ethylbenzene. Unexpected activity (EB conv.: 73%) and thermal stability (> 100 h on steam) at 450°C are observed. Such a facile synthetic strategy may inspire the fabrication of other types of HMCs for more specific tasks.

Transition metal carbides (TMCs) are an emerging class of active materials in various fields such as heterogeneous catalysis and energy-related processes (e.g., oxygen evolution reaction, hydrogen evolution reaction), because of their excellent electrical and thermal conductivities, earth–abundant feature, noble-metal-like surface reactivity and good chemical stability.[1-3] Being superior to mono-metal carbide, incorporating another hetero–metal cation into an ordered lattice could modify the corresponding electronic, thermal and chemical properties for target processes.[4,5] Therefore, many binary ternary TMCs have recently been prepared *via* multi–step synthetic procedures, meanwhile improved intrinsic activity were often observed in a wide range of catalytic processes.[6,7] However, the thermal stability of current TMCs is still far from ideal, since the growth and aggregation of active carbide particles usually occur in high-temperature (e.g., 400-600°C) catalysis, leading to a significant loss of catalytic activity.

Just recently, high–entropy crystalline materials (e.g., metal oxides,[8,9]metal diborides,[10] and metal nitrides[11]) that contain five or more metal elements at appr. equal ratios in single-phase solid solution, have attracted significant attention because of their exceptional entropic properties, including improved thermal/chemical stability.[12-14] It is understandable that the increase of metal components randomly doped in pristine cation lattice would contribute to a higher entropy.[15,16] From the equation of Gibbs free energy (ΔG= ΔH-TΔS), a more negative free energy value could be expected for the high-entropy materials working at higher temperature. In other words, entropy-stabilized TMC in principle could resist the sintering during high temperature catalysis. For example, Pt/Ru@(NiMgCuZnCo)O_x, showed good stability at high temperature (e.g., 500°C) hydrogenation of atmospheric CO_2 to CO.[17]

However, the design of high–entropy metal carbides (HMCs) is challenging, because multi metal cations with different ionic radiusand coulomb force are usually immiscible in a single solid solution. Toward this end, we moved our attention to Poly(ionic liquids) (PILs), which is a kind of ionic carriers resulting from the polymerization of ionic liquids (IL) monomers.[18-21] Interestingly, the coordination of PIL/IL with metal salts would produce homogeneous metal-containing ionic compounds, such as [EMIM][MBr_x] (EMIM: 1-ethyl-3-methylimidazolium), [EMIM][MCl_x], Poly[Ph-Py]-[$CuCl_2Br$].[23,24] Theoretically, PILs could store metal ions by coordination, at the same time PILs as ion matrixes may promote the flowand dispersion of metal ion.[19,24,25] In principle, those properties of PIL may be beneficial for the formation of a single phase HMCs by avoiding phase separation during calcination.

Herein, by the PIL–assisted assembly strategy, we prepared HMC nanoparticles (NPs), that are composed of five homogeneously dispersed metals (Mo, W, Nb, V, Cr). Those HMC NPs were in-situ incorporated on nitrogen-doped carbon (NC) (HMC@NC-*t*, *t* stands for the pyrolysis temperature) during pyrolysis. The high entropy feature endows HMC@NC-900 improved catalytic activity (EB conv.: 73%) and stability (> 100 h on steam) in the dehydrogenation of

a The Key Laboratory of Synthetic and Biological Colloids, Ministry of Education, School of Chemical and Material Engineering, Jiangnan University, Wuxi 214122, Jiangsu, China
b Department of Chemistry, University of Tennessee, Knoxville, TN 37996, USA
c School of Chemistry and Chemical Engineering, Shanghai Jiao Tong University, Shanghai 200240, P. R. China. E-mail: chemistryzpf@sjtu.edu.cn
d Chemical Sciences Division, Oak Ridge National Laboratory Knoxville, TN 37831, USA. E-mail: dais@ornl.gov
† Footnotes relating to the title and/or authors should appear here.
Electronic Supplementary Information (ESI) available: [details of any supplementary information available should be included here]. See DOI: 10.1039/x0xx00000x

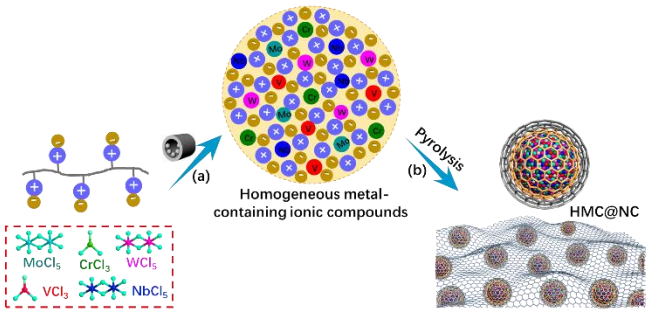

Scheme 1. Schematic illustration of the PIL-assisted strategy for the synthesis of HMC nanoparticles on nitrogen-doped carbon.

ethylbenzene (EB), in comparison with the monometallic metal catalysts (e.g., MoC).

As a regular and readily available PIL, poly(3–cyano–1–vinylimidazolium bromide) ([PCIM]Br) was first selected as the metal cation carrier and carbon source for the preparation of HMC@NC-*t*. Meanwhile, metal ions including Mo(Ⅴ), W(Ⅴ), Nb(Ⅴ), Zr(Ⅳ), Ti(Ⅳ), Ta(Ⅴ), Hf(Ⅳ), V(Ⅲ or Ⅴ), or Cr(Ⅲ) were considered as metal sources, because those cations could be individually used for the synthesis of metal carbides. The electrostatic assembly of an equimolar mixture of five transition–metal chlorides (MCl_x) and [PCIM]Br was performed via solid-state ball milling to form ionic hybrids [PCIM]Br-MCl_x. After carbonization in nitrogen (N_2) at 600-900°C, the HMC@NC-*t* was obtained (**Scheme 1**). For comparison, carbide samples containing single or four metals were also prepared by such a method.

The crystal phase of the obtained samples was investigated by X-ray diffraction (XRD). Typically, the XRD patterns show the phase evolution of [PCIM]Br-MCl_x (M = Mo,W, V, Cr, and Nb) calcined from 600 to 900°C (**Figure 1A**). No peak was observed at 600°C, demonstrating an amorphous structure. Prominent phases came into being when the pyrolysis temperature was 700°C, and four distinct diffraction peaks at 36.5°, 42.4°, 61.5°, and 74.7° appeared at 800°C. The higher carbonization temperature of 900°C resulted in significantly increased peak intensity, arguing for a higher crystallinity degree for HMC@NC-900 sample. The average particle size of HMC calculated by Scherrer's equation was ~3.8 nm. A careful comparison to those of five typical carbides (MoC, WC, NbC, VC, CrC) suggests the formation of single-phase structure by current HMC. Its four peaks in XRD were similar to those by (111), (200), (220), and (311) planes of cubic phase molybdenum carbide (MoC) (JCPDS Card No. 65-0280) (**Figure S1**). X–ray photoelectron spectroscopy (XPS) was further performed, and the high-resolution spectra of Mo 3d, W 4f, Nb 3d, Cr 2p, and V 2p display the characteristic peaks for metal-carbon bond. Thus, the XPS results confirm the formation of five–metallic carbides in HMC@NC-900 (**Figure S2**).

To elucidate the lattice packing of HMC@NC-900, a geometrical energy minimization by using the Materials Studio Software package based on the *Fm-3m* topology model of $Mo_{0.2}W_{0.2}V_{0.2}Cr_{0.2}Nb_{0.2}C$ was performed, and the unit cell parameters were determined (**Figure 1B**). The HMC@NC-900 model exhibited cubic unit cells with a = b = c = 4.28 Å, α = β = γ =90°. Moreover, the Rietield refinement offered a simulated XRD pattern, which is in good agreement with the experimental pattern, as suggested by their tiny difference. The final wRp and Rp values were 1.95% and 1.54%, respectively. This result in turn indicates that five hetero–metal cations were uniformly incorporated into an ordered carbide lattice, forming a single cubic phase HMC (**Figure 1C-1D**).

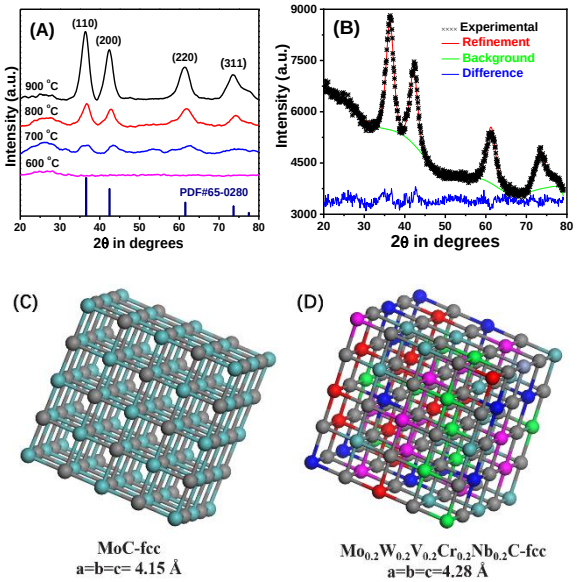

Figure 1.(A) XRD patterns of HMC@NC pyrolyzed at 600, 700, 800, and 900 °C, respectively; (B) XRD patterns of $Mo_{0.2}W_{0.2}V_{0.2}Cr_{0.2}Nb_{0.2}C$ with the observed profile in black, refined in red, background in green, and the difference (observed minus refined) in blue; (C) Structural view of MoC.(D) Structural view of $Mo_{0.2}W_{0.2}V_{0.2}Cr_{0.2}Nb_{0.2}C$.

Interestingly, the carbonization of four metal precursors also resulted in the formation of single–phase metallic carbides, as shown by their similar XRD patterns with $Mo_{0.2}W_{0.2}V_{0.2}Cr_{0.2}Nb_{0.2}C$ (**Figure S3**). However, their XRD intensity is weaker than that by $Mo_{0.2}W_{0.2}V_{0.2}Cr_{0.2}Nb_{0.2}C$. It seems reasonable if a more negative Gibbs-free energy is considered with the addition of another metal species. By using NH_4VO_3 to replace VCl_3 for the synthesis of HMC@NC-900, single–phase high entropy materials can also be achieved (**Figure S4**). However, when tetravalent metal ions, like Zr(Ⅳ), Ti(Ⅳ), Ta(Ⅴ), or Hf(Ⅳ), were introduced into the [PCIM]Br-MCl_x precursors, they tend to create phase–separated metallic carbides, as indicated by XRD patterns in **Figure S5**. These observations demonstrate that tetravalent metal ions are difficult to be incorporated into an uniform carbide lattice. It is probably because of their completely different chemical affinity, valence states, and lattice types to those of metal atoms in HMC@NC-900.[26]

To investigate the effect of carbon sources for the HMC formation, various PILs were prepared and used as control carbon precursors. Similar to that of [PCIM]Br, poly(3–butyl–1–vinylimidazolium bromide) ([PBIM]Br), poly(1–cyano–4–vinylpyridine bromide) ([PCPy]Br), and 3–cyano–1–vinylimidazoliumbromide monomer ([CIM]Br), all allowed the generation of single cubic phase HMCs, albeit with lower crystallinity degree as revealed by XRD patterns (**Figure 2A)**. In contrast, MCl_x mostly converted into metal oxides when using [PCIM]BF_4 or [PCIM]DCD (DCD denotes dicyandiamide anion) as carbon source. TMCs have been synthesized using neutral poly(vinyl pyrrolidone) or imidazole as carbon sources.[27,28] However, these compounds tend to create phase–separated metallic carbides in the present multiple-metal system, as indicated by XRD patterns in

Figure S6. All control processes suggest the key role of Br anions for the formation of HMCs.

The unique feature of Br–based PILs for producing HMCs can be attributed to their good coordination capacity for MCl_x.[29,30] Actually, metal-containing ionic liquids with halometalate ions (e.g., [EMIM][MBr_x], [EMIM][MCl_x]) and the corresponding polymers (e.g., Poly[Ph-Py]-[$CuCl_2Br$], PILM-Cu, PILM-Fe) have been well studied in ionic liquid community.[22,23] To explore this hypothesis, the XRD pattern of [PCIM]Br-MCl_x mixture was measured. A wide peak around 26° was observed in XRD pattern and the strong response of metal chlorides disappeared (**Figure 2B**). This result suggests the change from crystalline MCl_x to amorphous [PCIM]Br-MCl_x ionic hybrid. Thus, cation carrier behavior of [PCIM]Br may drive metal ions "movement" and "fusion" to form a homogeneous precursor during the pyrolysis process, which was subsequently transferred to crystalline single–phase HMC embedded within NC matrices.

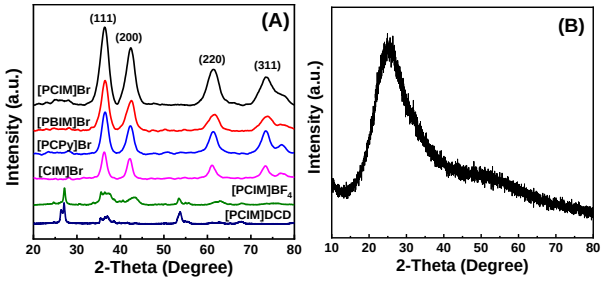

Figure 2. (A) XRD patterns for HMC@NC pyrolyzed at 900°C with different carbon sources; (B) XRD pattern for [PCIM]Br-MClx mixture

The porosity of the obtained samples was examined by N_2 sorption isotherm at 77 K (**Figure S7**). All samples derived from Br–based PILs at 900°C were proved to be microporous materials, as significant N_2 uptakes were observed at low relative pressure (e.g., P/P_0<0.05) (**Table S1** and **Figure S8**). Thespecific surface areas were in the range of 58–278 m^2/g. [PCIM]Br and [CIM]Br with –C≡N functional groups caused higher specific surface areas (~270 m^2/g) than [PBIM]Br (133 m^2/g) and [PCPy]Br (58 m^2/g) did, which suggests that –C≡N functionalized imidazole is more beneficial for the formation of abundant porous NC structure. Interestingly, the N_2 adsorption curve of HMC@NC-800 material afforded an increasing uptake at P/P_0=~0.6–0.8, and the pore size distribution located in the range of mesopores, centered at 8 nm.

To inquire the carbonization process, thermogravimetric analysis (TGA) from room temperature to 900 °C in air was carried out (**Figure S9**). A weight loss of about 40% between 350–450°C was observed, indicating that the porosity of HMC@NC-900 mainly comes from the decomposition of the PILs. Two characteristic peaks of D band (1314 cm^{-1}) and G band (1590 cm^{-1}) in the Raman spectroscopy (**Figure S10**) confirm the existence of graphitic carbon structure within HMC@NC-900. Both porous and graphitic structure of NC provide a useful matrix for the dispersion of HMCs.[31]

Scanning transmission electron microscopy (STEM) and transmission electron microscopy (TEM) were then performed to study the morphology of carbide samples. In general, HMC NPs are well dispersed on carbon matrices. The average sizes of HMC NPs were estimated to be ~4 nm (**Figure 3A,B**), in agreement with the broad peaks on XRD patterns. The lattice spacing of HMC NP is ~0.25 nm (**Figure 3C**), corresponding to (111) crystal plane of HMC phase. The fast Fourier transfer (FFT) pattern shows discontinuous diffraction rings. It can be indexed by a single–phase face centered cubic (fcc) structure (**Figure 3D)**, which matches well with the XRD results. Energy–dispersive X–ray spectroscopy (EDS) maps of HMC@NC-900 reveals homogeneous dispersion of Mo, W, Cr, V, and

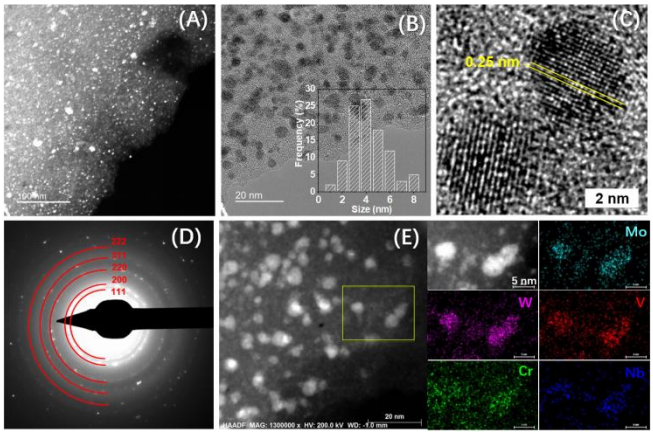

Figure 3. (A) STEM image, (B) TEM image,particle size distribution, (C) HR-TEM image, and (D) FFT pattern of HMC@NC-900; (E) EDS maps of Mo, W, Cr, V, and Nb in HMC@NC-900.

Nb over the entire domain in the range of several micrometers (**Figure S11**), demonstrating that HMC NPs in HMC@NC-900 are well dispersed. Notably, EDS maps at a nanometer level also display the well dispersion of five hetero–metal species, further confirming a single phase in HMC NPs(**Figure 3E**). Based on above results, it seems fair to say that HMCs have been successfully prepared in the form of NPs locating on porous carbon.

Styrene (ST) is an important monomer for synthetic polymers, but its production process through ethylbenzene (EB) dehydrogenation is still far from satisfactory.[32]The dehydrogenation of EB with CO_2 (CO_2-DEB) has been recognized as a potential process for the synthesis of ST. Much effort has been paid on the development of active and stable catalysts for CO_2-DEB,[33,34] but most of the known catalysts are quickly deactivated because of sintering or aggregation during high temperature catalysis. By combination of high-entropy phase, small particle size and high surface area, the HMC@NC-900 seems like a potential material for high temperature catalysis.

Then, CO_2-DEB was selected as a model reaction to evaluate the catalytic performance of HMC@NC-900. Under the conditions of P_{CO2} = 0.1 MPa, CO_2/EB molar ratio = 5, and the flow rate of EB = 0.02 mL min^{-1}, the effect of reaction temperature on the EB conversion and ST selectivity is displayed in **Figure S12A**. When the reaction temperature increased from 350 to 550°C, the maximum EB conversion of ~73% with ST selectivity of ~95% was achieved at 450°C. However, the monometallic Mo_2C@NC was less active than HMC@NC-900, only offering a EB conversion of ~40% at 500°C. Actually, the HMC@NC-900 catalyst affords higher or comparable activity, compared with the state-of-art metal oxide catalysts, such as MnO_x[33], VO_x/Al_2O_3[34], CeO_2-HAS[35], V_2O_5–$Ce_{0.5}Zr_{0.5}O_2$–Al_2O_3[36]. Compared with the pure ceramics, the formation of multi-metallic ceramic solid solution is known to create more defects and more negative Gibbs free energy,[37] which may modify the catalytic efficiency. Besides, the high dispersion of small HMC NPs and rich

porosity of NC can maximally expose active sites and accelerate mass transfer, thereby contributing to the good activity.

The stability test for EB dehydrogenation was performed at 450°C (**Figure S12B**). In the case of Mo_2C@NC, EB conversion significantly decreased from ~35% to ~22% within the initial 15 h, then it gradually declined. This might be attributed to the deposited coke over the catalyst during CO_2-DEB. In contrast, ~70% EB conversion was maintained with an invariant selectivity over HMC@NC-900 after running 100 h, demonstrating an excellent durability. Actually, well-dispersed HMC NPs were observed in the STEM-HAADF image of spent HMC@NC-900 catalyst (**Figure S13**). From the above results, one can conclude that the high-entropy structure of HMC@NC-900 led to improved thermal stability of catalyst, which might resist the coking/sintering during CO_2-DEB process at high temperature.

In summary, a facile PIL–assisted assembly strategy was introduced for the synthesis of porous NC–encapsulated HMC nanoparticles (NPs) containing five homogeneously dispersed metals (Mo, W, Nb, V, Cr) (HMC@NC). The resulting HMC@NC-900 displayed crystalline high-entropy phase, small particle size (~4 nm), and high porosity with a surface area of ~270 m^2/g. These structural patterns and properties endow HMC@NC-900 with unexpected activity (EB conv.: 73%) and thermal stability (> 100 h on steam) in dehydrogenation of ethylbenzene (EB) with CO_2, much higher than that of monometallic molybdenum carbide (Conv.: 41%). The present methodology for preparing HMCs may be extended to the design and synthesis of more attractive high-entropy ceramics for more high-temperature catalysis, such as dehydrogenation of alkanes and CO_2 reduction.

The authors thank the National Natural Science Foundation of China (no. 21978115). S. D. And H. C. were supported by the Division of Chemical Sciences, Geosciences and Biosciences, Office of Basic Energy Sciences, U.S. Department of Energy. P. F. Z. acknowledges National Natural Science Foundation of China (Grant No. 21776174), Shanghai Rising-Star Program (20QA1405200), Shanghai Jiao Tong University Scientific and Technological Innovation Funds (No.2019QYB06), and National Key R & D Plan (2020YFB0606400) for their support.

There are no conflicts to declare.

Notes and references

1 X. Zhang, X. B. Zhu, L. L. Lin, S. Y. Yao, M. T. Zhang, X. Liu, X. P. Wang, Y. W. Li, C. Shi, D. Ma,*ACS Catal.***2016**, *7*, 912-918.

2 S. T. Hunt, M. Milina, A. C. Alba-Rubio, C. H. Hendon, J. A. Dumesic, Y. Román-Leshkov,*Science***2016**,*352*, 974-978.

3 S.Li, C.Cheng, A.Sagaltchik, P.Pachfule,C. Zhao, A.Thomas, *J. Am. Chem. Soc.***2019**,*139*, 11989-11997.

4 Z. M. Cui, Y. T. Li, G. T. Fu, X. Li,J. B. Goodenough,*Adv. Mater.***2017**,*29*, 1702385.

5 H. Fashandi, M. Dahlqvist, J. Lu, J. Palisaitis, S. I. Simak, I. A. Abrikosov, J. Rosen, L. Hultman, M. Andersson, A. L. Spetz, P. Eklund,*Nat. Mater.***2017**, *16*, 814-819.

6 H. S. Fan, H. Yu, Y. F. Zhang, Y. Zheng, Y. B. Luo, Z. F. Dai, B. Li, Y. Zong, Q. Y. Yan, *Angew.Chem., Int. Ed.***2017**, *129*, 12740 – 12744.

7 D. A. Hardy, E. T. Nguyen, S. E. Parrish, E. A. Schriber, L. Schlicker, A. Gili, F. Kamutzki, J. N. Hohman, G. F. Strouse,*Chem. Mater.***2019**, *31*,8163-8173.

8 A. Sarkar, L. Velasco, D. Wang, Q. S. Wang, G. Talasila, L. Biasi, C. Kübel, T. Brezesinski, S. S. Bhattacharya, H. Hahn,B. Breitung,*Nat.Commun.***2018**, *9*, 3400.

9 D. Berardan, S. Franger, A. K. Meena, N. Dragoe,*J. Mater. Chem. A***2016**, *4*, 9536–9541.

10 J. Gild, Y. Y. Zhang, T. Harrington, S. C. Jiang, T. Hu, M. C. Quinn, W. M. Mellor, N. X. Zhou, K. Vecchio, J. Luo,*Sci. Rep.***2016**, *6*, 37946.

11 T. Jin, X. H. Sang, R. R. Unocic, R. T. Kinch, X. F. Liu, J. Hu, H. L. Liu,S. Dai,*Adv. Mater.***2018**, *30*, 1707512.

12 A. Sarkar, Q. Wang, A. Schiele, M. R. Chellali, S. S. Bhattacharya, D. Wang, T. Brezesinski, H. Hahn, L. Velasco, B. Breitung, *Adv. Mater*. **2019**, *31*, 1806236.

13 Q. Wang, A. Sarkar, D. Wang, L. Velasco, R. Azmi, S. S. Bhattacharya, T. Bergfeldt, A. Duvel, P. Heitjans, T. Brezesinski, H. Hahn, B. Breitung, *Energy Environ. Sci.***2019**, *12*, 2433-2442.

14 T.Wang, H.Chen, Z.Yang, J.Liang, S.Dai, *J. Am. Chem. Soc.***2020**,*142*, 4550-4554.

15 P.Sarker, T.Harrington, C.Toher, C.Oses, M.Samiee, J. P.Maria, and S.Curtarolo, *Nat. commun.***2018**,*9*, 1-10.

16 Y. G. Yao, Z. N. Huang, P. F. Xie, S. D. Lacey, R. J. Jacob, H. Xie, F. J. Chen, A. Nie, T. C. Pu, M. Rehwoldt, D. W. Yu, M. R. Zachariah, C. Wang, R. Shahbazian-Yassar, J. Li, L. B. Hu,*Science***2018**, *359*, 1489–1494.

17 H. Chen, W. Lin, Z. Zhang, K. Jie, D. R. Mullins, X. Sang, S. Yang, C. J Jafta, C. A. Bridges, X. Hu, R. R. Unocic, J. Fu, P. Zhang, S. Dai, *ACS Mater. Lett*. **2019**, *1*, 83-88.

18 W. J. Qian, J. Texter, F. Yan,*Chem. Soc. Rev.***2017**,*46*, 1124-1159.

19 M. Antonietti, D. Kuang, B. Smarsly, Y. Zhou, *Angew. Chem. Int. Ed*. **2004**, *43*, 4988-4992.

20 J. Yuan, D. Mecerreyes, M. Antonietti; *Progress in Polymer Science***2013**, *38*, 1009-1036.

21 J. Yuan, M. Antonietti, *Polymer***2011,***52*, 1469-1482.

22 H. Niedermeyer, J. P. Hallett, I. J. Villar-Garcia, P. A. Hunt, T. Welton,*Chem. Soc. Rev.***2012**, *41*, 7780–7802.

23 Z. Q. Zheng, J. N. Guo, H. L. Mao, Q. M. Xu, J. Qin, F. Yan,*ACS Biomater. Sci. Eng.***2017**, *3*,922-928.

24 M.Watanabe, M. L.Thomas, S.Zhang, K.Ueno, T.Yasuda, andK.Dokko, *Chem. Rev.***2017**,*117*, 7190-7239.

25 D. R.MacFarlane, M.Forsyth, P. C.Howlett, M.Kar, S.Passerini, J. M.Pringle, and S.Zhang, *Nat. Rev. Mater.***2016**,*1*, 1-15.

26 R.Zhang, X.Huang,D. Wang, T. K.Hoang, Y.Yang, X.Duan, andG. Wen, *Adv. Funct. Mater.***2018**,*28*, 1705817.

27 Y. J. Oh,J. H. Kim, J. Y. Lee,S. K. Park,Y. C. Kang,*Chem. Eng. J. Chem. Eng. J.***2020**,*384*, 123344.

28 H. B. Wu,X. W. D. Lou,*Sci. Adv.***2017**, *3*, 9252.

29 P. Wasserscheid,W. Keim,*Angew. Chem., Int. Ed.***2000**, *39*, 3772-3789.

30 L. Y. Sun, J. F. Brennecke,*Ind. Eng. Chem. Res.***2015**, *54*, 4879-4890.

31 M. Titirici, R. J. White, N. Brun, V. L. Budarin, D. S. Su, F. del Monte, J. H. Clark, M. J. Maclachlan, *Chem. Soc. Rev*. **2015**, *44*, 250-290.

32 M.B. Ansari, S.E. Park,*Energy Environ. Sci.***2012**,*5*, 9419–9437.

33 K. Ren, J. Song, Y. H. Song, H. Wang, Z. H. Liu, Z. T. Liu, J. Q. Jiang, Z. W. Liu, *J. CO_2 Util.***2017**, *22*, 63–70.

34 G. Q. Yang,H. Wang,T. Gong,Y. H. Song,H. Feng,H. Q. Ge,H. B.Ge,Z. T. Liu,Z. W. Liu,*J. Catal.***2019**, *380*, 195-203.

35 L. Zhang, Z. Wu, N. C. Nelson, A. D. Sadow, I. I. Slowing, S. H. Overbury, *ACS Catal*. **2015**, *5*, 6426-6435.

36 H. Wang, W. Zhu, G. Yang, Y. Zhang, Y. Song, N. Jiang, Z. Liu, Z. Liu, *Ind. Eng. Chem. Res*. **2019**, *58*, 21372-21381.

37 Y. W. Zhang, G. M. Stocks, K. Jin, C. Y. Lu, H. B. Bei, B. C. Sales, L. M. Wang, L. K. Beland, R. E. Stoller, G. D. Samolyuk, M. Caro, A. Caro, W. J. Weber,*Nat.Commun.***2015**, *6*, 8736.

